

Design and fabrication of GeAsSeS chalcogenide waveguides with thermal annealing

Limeng Zhang(张李萌), Jinbo Chen(陈锦波), Jierong Gu(顾杰荣), Yixiao Gao(高一骁), Xiang Shen(沈祥), Yimin Chen(陈益敏), and Tiefeng Xu(徐铁峰)

Citation: Chin. Phys. B, 2021, 30 (**3**): 034210. DOI: 10.1088/1674-1056/abd757
Journal homepage: http://cpb.iphy.ac.cn; http://iopscience.iop.org/cpb

What follows is a list of articles you may be interested in

Effect of dark soliton on the spectral evolution of bright soliton in a silicon-on-insulator waveguide

Zhen Liu(刘振), Wei-Guo Jia(贾维国), Hong-Yu Wang(王红玉), Yang Wang(汪洋), Neimule Men-Ke(门克内木乐), Jun-Ping Zhang(张俊萍)

Chin. Phys. B, 2020, 29 (**6**): 064212. DOI: 10.1088/1674-1056/ab84d9

Extraordinary propagation characteristics of electromagnetic waves in one-dimensional anti-*PT*-symmetric ring optical waveguide network

Jie-Feng Xu(许杰锋), Xiang-Bo Yang(杨湘波), Hao-Han Chen(陈浩瀚), Zhan-Hong Lin(林展鸿)

Chin. Phys. B, 2020, 29 (**6**): 064201. DOI: 10.1088/1674-1056/ab8371

Propagation characteristics of parallel dark solitons in silicon-on-insulator waveguide

Zhen Liu(刘振), Weiguo Jia(贾维国), Yang Wang(汪洋), Hongyu Wang(王红玉), Neimule Men-Ke(门克内木乐), Jun-Ping Zhang(张俊萍)

Chin. Phys. B, 2020, 29 (**1**): 014203. DOI: 10.1088/1674-1056/ab577d

Extraordinary transmission and reflection in *PT*-symmetric two-segment-connected triangular optical waveguide networks with perfect and broken integer waveguide length ratios

Jia-Ye Wu(吴嘉野), Xu-Hang Wu(吴栩航), Xiang-Bo Yang(杨湘波), Hai-Ying Li(李海盈)

Chin. Phys. B, 2019, 28 (**10**): 104208. DOI: 10.1088/1674-1056/ab3f92

Design of an augmented reality display based on polarization grating

Renjie Xia(夏人杰), Changshun Wang(王长顺), Yujia Pan(潘雨佳), Tianyu Chen(陈天宇), Ziyao Lyu(吕子瑶), Lili Sun(孙丽丽)

Chin. Phys. B, 2019, 28 (**7**): 074201. DOI: 10.1088/1674-1056/28/7/074201

Design and fabrication of GeAsSeS chalcogenide waveguides with thermal annealing*

Limeng Zhang(张李萌)[1], Jinbo Chen(陈锦波)[1], Jierong Gu(顾杰荣)[2], Yixiao Gao(高一骁)[1], Xiang Shen(沈祥)[1,†], Yimin Chen(陈益敏)[3,‡], and Tiefeng Xu(徐铁峰)[1,2]

[1] *Laboratory of Infrared Materials and Devices & Key Laboratory of Photoelectric Detection Materials and Devices of Zhejiang Province, Research Institute of Advanced Technology, Ningbo University, Ningbo* 315211, *China*

[2] *Ningbo Institute of Oceanography, Ningbo* 315832, *China*

[3] *Department of Microelectronic Science and Engineering, School of Physical Science and Technology, Ningbo University, Ningbo* 315211, *China*

(Received 15 October 2020; revised manuscript received 22 December 2020; accepted manuscript online 30 December 2020)

We reported a chalcogenide glass-based rib waveguide fabricated using photolithography and dry etching method. A commercial software (COMSOL Multiphysics) was used to optimize the waveguide structure and the distribution of the fundamental modes in the waveguide based on the complete vector finite component. We further employed thermal annealing to optimize the surface and sidewalls of the rib waveguides. It was found that the optimal annealing temperature for GeAsSeS films is 220 °C, and the roughness of the films could be significantly reduced by annealing. The zero-dispersion wavelength (ZDW) could be shifted to a short wavelength around ∼ 2.1 μm via waveguide structural optimization, which promotes supercontinuum generation with a short wavelength pump laser source. The insertion loss of the waveguides with cross-sectional areas of 4.0 μm×3.5 μm and 6.0 μm×3.5 μm was measured using lens fiber and the cut-back method. The propagation loss of the 220 °C annealed waveguides could be as low as 1.9 dB/cm at 1550 nm.

Keywords: chalcogenide film, dispersion engineering, optical waveguide, thermal annealing

PACS: 42.82.–m, 42.82.Cr, 42.82.Et, 42.81.Dp **DOI:** 10.1088/1674-1056/abd757

1. Introduction

Supercontinuum (SC) generation is realized via dispersion and a series of nonlinear effects.[1] Broadband mid-infrared SC light source has been found to be applicable to optical coherence tomography, bio-imaging, molecular fingerprinting spectroscopy, and high precision frequency metrology.[2–5] Recently, SC generation has been widely studied in optical fiber as well as planar waveguide devices.[6,7] Generally, it requires the fiber or waveguide to be pumped at a waveguide close to its zero-dispersion wavelength in order to achieve the maximum expansion of the SC spectrum. In addition, it is preferable to choose materials with a large Kerr nonlinearity[8] since SC generation is typical nonlinear interaction processes including self-phase modulation, cross-phase modulation, soliton dynamics, Raman scattering, four-wave mixing, and so on.[9,10]

ChGs have emerged as promising nonlinear materials with a number of distinct properties that make them attractive for mid-IR applications, ChGs consist of one or more of chalcogen elements S, Se, and Te that are covalently bonded with glass forming materials such as As, Sb, Ge, and Ga.[11] Compared to other glass materials, ChGs exhibit higher optical Kerr nonlinearity, high refractive index, and wide mid-infrared transparency window.[12] ChGs can provide a wide infrared transmission spectrum with sulfides exceeding 8.5 μm, selenides up to 14 μm, and tellurites to around 20 μm. Silicon has some disadvantages in high-speed nonlinear optical signal processing. In 1550 nm band, silicon would be affected by two-photon absorption (TPA) and free carrier absorption (FCA), thereby reducing the performance.[13] Chalcogenide glasses are chosen because they have some unique properties, including low TPA and no FCA.[14–17] The third-order nonlinearity of ChGs up to $\sim 10^{-13}$ cm^2/W is 100–1000 times higher than that of silica.[18,19] Recently, Karim *et al*. reported a numerical study of the air clad $Ge_{11.5}As_{24}Se_{64.5}$ rib waveguide with a SC spanning from 2 μm to 6 μm when the waveguide was pumped with a peak power of 500 W at a wavelength of 3.1 μm.[20] Further theoretical studies by Karim have shown a supercontinuum output from 1.8 μm to beyond 8 μm in a $Ge_{11.5}As_{24}Se_{64.5}$ rib waveguide on MgF_2.[21] Zhang *et al*. reported SC spectrum ranging from 1 μm to 7 μm in As_2S_3 glass rib waveguide pumped by pulses with a peak power of 2 kW, and duration of 50 fs at a wavelength of 1.55 μm.[22] Moreover, Yu *et al.* also presented experimental results showing a linearly polarized SC spectrum extending from 2 μm to 10 μm over highly nonlinear rib waveguide employing 4.5 kW peak

*Project supported by the National Natural Science Foundation of China (Grant Nos. 61904091 and 61775111), Zhejiang Provincial Natural Science Foundation of China (Grant No. LR18E010002), the Natural Science Foundation of Ningbo City, China (Grant No. 2019A610065), the International Cooperation Project of Ningbo City, China (Grant No. 2017D10009), and K. C. Wong Magna Fund in Ningbo University, China.

†Corresponding author. E-mail: shenxiang@nbu.edu.cn

‡Corresponding author. E-mail: chenyimin@nbu.edu.cn

© 2021 Chinese Physical Society and IOP Publishing Ltd

power 330 fs pulses pumped at 4.184 μm.[7] The width of the SC spectrum generated in the planar chalcogenide waveguide is smaller than that in the fibers. However, the advantage of the waveguide platform is that all the functions can be integrated on a single chip, which can ultimately be used for more powerful lab-on-chip systems.[23]

In this paper, we fabricated $Ge_{11}As_{29}S_{25}Se_{35}$ waveguide by UV-lithography and dry etching, and determined appropriate etching parameters and thermal annealing temperature (220 °C) to reduce the scattering loss of the surface and sidewalls of the waveguide.[24,25] We chose $Ge_{11}As_{29}S_{25}Se_{35}$ glass component because the $Ge_{11.5}As_{24}Se_{64.5}$ (MCN≈ 2.67) component in the Ge–As–Se glass system has been demonstrated to be the most stable composition,[26] and the replacement of Se with a certain amount of S can significantly increase the laser damage threshold in Ge–As–Se glass system.[27] GeAsSeS glass exhibits relatively good thermal stability (T_g = 237 °C) and a third-order nonlinearity around 2.82–5.46×10^{-14} cm^2/W at 1550 nm.[14] The surface roughness of the as-deposited and annealed films, the morphologies, and the propagation loss of the waveguide were characterized. In addition, the two ChG materials are thermally matched which are highly suitable for preparing step-index waveguides.

2. Waveguide design and simulation

The waveguide structure was optimized by changing the height and width of the waveguide to obtain a good distribution of the optical modes. The rib waveguide was applied because it can effectively reduce the interaction between the mode and the sidewall of the waveguide, which is beneficial to the fabrication of low-loss waveguides. The optimized structure of the waveguide was obtained using a commercial software (COMSOL Multiphysics). The structure diagram of the waveguide is shown in Fig. 1. A 1.1 μm GeAsS film was deposited on a silicon (TOX) substrate with 2 μm thermal oxide layer by thermal evaporation, such a thin film could be used as the bottom cladding layer to reduce light leaks into the substrate. Then a 4.5 μm-thick GeAsSeS film with 3.5 μm etching depth was used as the optical transmission layer. Another layer of GeAsS was used to cover the top of the waveguide to prevent the core layer from absorbing moisture and other impurities in the air. The width of the waveguide was fixed at 2 μm, 4 μm, and 6 μm, respectively.

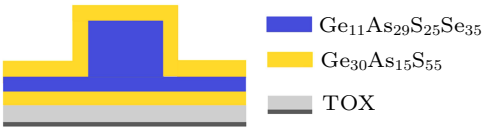


Fig. 1. Schematic of the waveguide cross section.

Figure 2 show the electric field distributions at different wavelengths. Figures 2(a) and 2(b) show the electric field distributions of quasi-TE and quasi-TM modes at 1550 nm, respectively. It is evident that quasi-TE and quasi-TM modes are well confined in the waveguide. The field distributions of the quasi-TE mode at wavelengths of 2 μm, 4 μm, 6 μm, and 8 μm in the waveguide are shown in Fig. 2(c). We found that even at long wavelengths, the mode field could be effectively confined in the rib structure. The width and height of the designed waveguide are 6 μm and 3.5 μm, respectively.

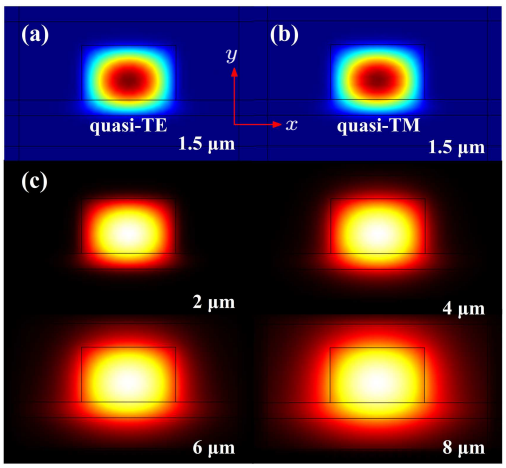


Fig. 2. (a) and (b) Electrical field distributions of the quasi-TE and quasi-TM modes at 1550 nm. (c) Electric field distribution of the quasi-TE mode at 2 μm, 4 μm, 6 μm, and 8 μm, respectively.

For ChG glass, the ZDW is usually larger than 4.5 μm, reducing the ZDW of the waveguide structure is crucial for SC applications,[28] since most of the commercially available lasers operate at short pump wavelengths less than 2 μm. The ZDW of the waveguide could be shifted to a shorter wavelength through dispersion engineering. The dispersion curves of the two modes are calculated by

$$D_W = \frac{\lambda}{c}\frac{d^2 n_{eff}}{d\lambda^2}. \quad (1)$$

The dispersion of the transmission mode is determined by the wavelength λ and the speed of light c, as well as the second derivative of the mode effective index (n_{eff}) relative to the wavelength. The calculated results of the designed waveguides with different widths are shown in Fig. 3. It can be seen from Fig. 3(a) that a 2 μm wide waveguide exhibits a close double-zero dispersion point, which limits the broadening of SC. Although in the short wavelength region, for 4 μm and 6 μm wide waveguides, quasi-TE and quasi-TM have almost the same influence on the dispersion of the waveguide. However, it is obvious that the effect of the quasi-TE mode on the waveguide dispersion is smaller than that of the quasi-TM mode as the wavelength increases. The ZDW of the quasi-TE mode and the quasi-TM mode in waveguides with widths of 4 μm and 6 μm is around 2.1 μm, which is shorter than the

ZDW reported in Refs. [29–31] The effective mode area (A_{eff}) is given by

$$A_{\text{eff}} = \left[\iint |E|^2 \,\mathrm{d}s\right]^2 \Big/ \iint |E|^4 \,\mathrm{d}s, \tag{2}$$

where E represents the electric field transverse component propagating inside the waveguide. The integration is performed on the whole waveguide cross-section calculation region. The A_{eff} of the waveguide with 6 μm width (14.3 μm^2 for TE mode and 14.5 μm^2 for TM mode) is obviously larger than that of the waveguide with 4 μm width (9.6 μm^2 for TE mode and 9.9 μm^2 for TM mode). The smaller the A_{eff}, the higher the nonlinear coefficient of the waveguide, which can enhance the nonlinear effect.

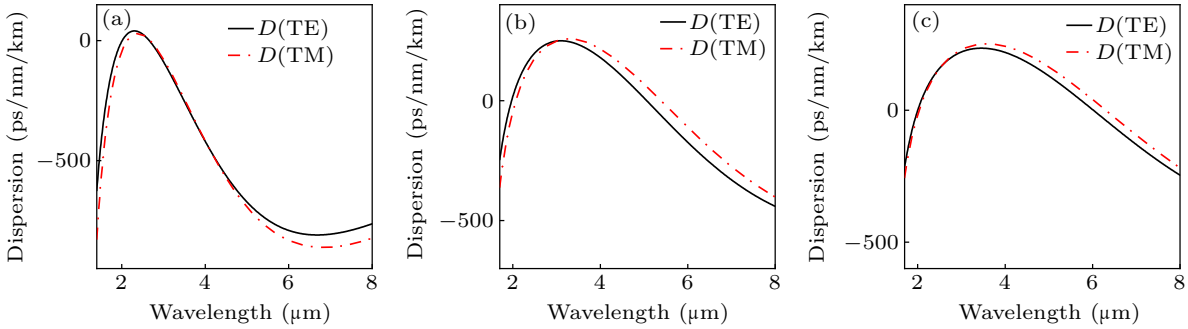


Fig. 3. Calculated dispersion curves of the quasi-TE and quasi-TM modes with the waveguide width of 2 μm, 4 μm, and 6 μm, respectively.

3. Waveguide fabrication

The GeAsSeS and GeAsS targets were fabricated using melting-quench method and then used as the source materials for the thermal evaporation. Figure 4 displays the flow chart of the fabrication process of the chalcogenide waveguide. 1.1 μm thick $Ge_{30}As_{15}S_{55}$ and 4.5 μm thick $Ge_{11}As_{29}S_{25}Se_{35}$ chalcogenide films were deposited on a TOX substrate successively. The films were annealed at 220 °C for 3 hours to reduce residual stress and scattering loss.[32] GeAsSeS waveguides were fabricated through UV-lithographic patterning and dry etching by employing a positive AZ series photoresist.[33] The photoresist with a thickness of 1–2 μm was spin-coated on the film and then the film was baked for 6 min at 90 °C to survive development and subsequent etching without peeling. After UV exposure, the photoresist was developed followed by hard baking. After a contact ultraviolet lithography for 8 s, the photoresist was developed followed by 0.5 h post-baking at 120 °C. During etching, the ICP power was 500 W, HF was 100 W, the reaction chamber pressure was 6 mTorr, and the etch rate was ∼ 1600 nm/min. The optimized CHF_3:CF_4 etching ratio allowed us to obtain a rib waveguide with smooth surface and high sidewall verticality. Finally, a 1 μm-thick GeAsS layer was covered as a protective layer on the core layer.

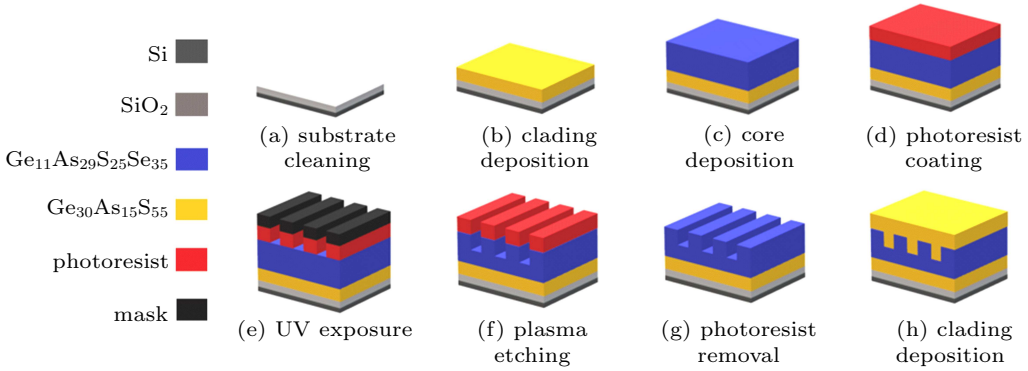


Fig. 4. Schematic fabrication process of the waveguide.

4. Results and discussion

The composition of the films was measured by using energy-dispersive x-ray spectroscopy (EDX). The refractive index curves of the $Ge_{11}As_{29}S_{25}Se_{35}$ and $Ge_{30}As_{15}S_{55}$ films are shown in Fig. 5. The linear refractive indexes of the films annealed at different temperatures below T_g (237 °C) were measured by an ellipsometer (J. A. Woollam IR-Vase II). Compared with $Ge_{18}Se_{82}$ and As_2S_3 films,[34,35] GeAsSeS films show the better stability of refractive index. The difference in refractive index between the annealed film and the deposited film is less than 0.04 in Fig. 5(b). The increase in refractive index caused by the densification of the film could be

explained by the increase in the number of heteropolar bonds after annealing, thereby increasing the effective polarizability of the material. The film thickness shows the opposite trend, i.e., it decreases with the annealing temperature. By raising the temperature to reach 240 °C, the film thickness drops sharply by ∼ 7 % due to the high temperature causing the material to evaporate from the surface, which is also reflected by the increase in surface roughness.

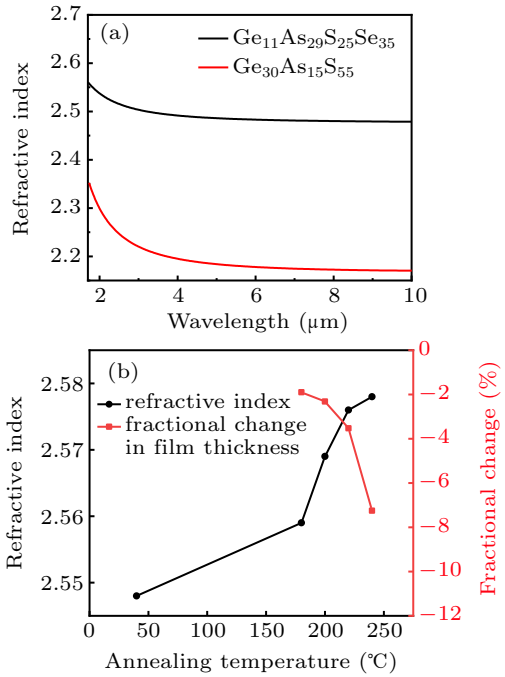


Fig. 5. (a) Refractive index of as-deposited films. (b) Variation in relative thickness and refractive index at 1550 nm of GeAsSeS films annealed at different temperatures.

The first and crucial step in low-loss waveguide fabrication is to prepare high quality films with stable physical properties. The glass material needs to be added several times during thermal evaporation coating, which would cause delamination of the film. Thermal annealing is a simple method to accelerate the relaxation of the film to its equilibrium state. The density of the film could be improved by the proper thermal annealing.[36] In Fig. 6, the morphology AFM images for the as-deposited and annealed GeAsSeS films show the fine particles on the surfaces of the films. Each group is processed with identical fabrication schemes but with different temperatures below T_g (237 °C). By performing thermal annealing treatment on the as-deposited film at a temperature from 180 °C to 240 °C with a step of 20 °C (Table 1), the change in root mean square roughness (RMS) of the film surface was measured by AFM. For the as-deposited film, the RMS is 2.98 nm and decreases with the increased temperature up to 220 °C, although the change is not obvious. The mean square error (MSE) decreases significantly as the temperature increases to 220 °C. The measurement results show that the roughness of the film annealed at 220 °C is reduced by 18% compared to that of the as-deposited film. By raising the temperature to over 240 °C, small cracks and bubbles were observed in the film through a microscopy, which is attributed to the thermal mismatch between the film and the silicon-based substrate. We thus conclude that the best thermal annealing temperature is 220 °C. The previous studies have shown that an annealing treatment can reduce the Rayleigh scattering of the films via the suppression of homopolar bonds, voids, and dangling bonds in the deposited film.[35] Compared with the as-deposited state, the annealing treated film has smaller nanoparticles, and thus could be used to prepare low-loss waveguides.

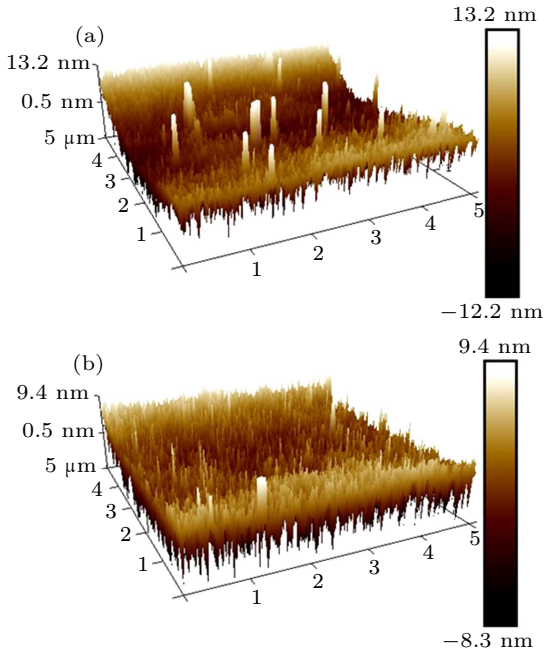


Fig. 6. AFM topographical image of Ge–As–Se–S film surfaces taken at 5×5 μm scanning area: (a) as-deposited film, (b) 220 °C annealed film.

Table 1. Surface amplitude parameter for GeAsSeS films.

Temperature	As-deposited	180 °C	200 °C	220 °C	240 °C
RMS (nm)	2.98	2.87	2.65	2.43	2.49
MSE (nm)	0.491	0.479	0.434	0.201	0.260

To obtain high-quality GeAsSeS waveguides, we chose a mixed gas of CF_4 and CHF_3 for etching. The gases in the reaction chamber of ICP form a plasma including ions, molecular mixtures, electrons, CF_x ($x = 1, 2, 3$) groups, and fluorine radicals. The main factor affecting the etching behavior is the relative density of the fluorine radicals. The etching strength increases as the density of fluorine radicals rises. The inert fluorocarbon polymer formed by the CF_x groups is deposited on the surface and sidewalls of the etched film. This fluorocarbon polymer protective layer can prevent further etching by fluorine radicals. Although the fluorocarbon polymer deposition and fluoride radical etching are isotropic, the lateral etching rate is lower than the vertical polymer removal rate. Enhanced anisotropy can reduce the occurrence of trenches and sidewall cuts in lateral etching.[37] We have previously tried using CF_4

and O_2 as etching gases, but some undesirable phenomena occurred, such as rough etched surfaces, curved sidewalls, and large etching deviation, due to a large number of fluorine radicals and relatively few CF_x groups in the etching environment.

Scanning electron microscopy (SEM) and optical microscopy were used to observe the morphology of GeAsSeS waveguides. It can be seen from Figs. 7(a) and 7(b) that the waveguide fabricated by the preparation process herein exhibits a vertical sidewall and excellent morphology. The vertical sidewalls of the rib waveguide can reduce the loss due to scattering and effectively confine the light in the mode field. Figures 7(c) and 7(d) show the cross-sectional morphology of the waveguide prepared by the as-deposited film and the annealed film. The waveguide prepared by the 220 °C annealed film exhibits better compactness on all levels, which is beneficial to the subsequent preparation of the waveguide without the problem of falling off.

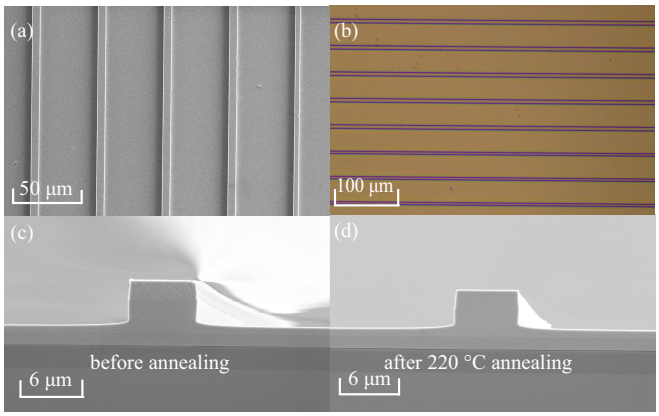


Fig. 7. (a) SEM image of the waveguide. (b) Optical microscopy image of the waveguide. (c) and (d) Cross-sectional view images of GeAsSeS rib waveguide before and after annealing.

The transmission properties of the waveguide samples were measured using an automated alignment system with lens fibers to couple light into and out of the waveguide and the output light was detected using a power meter (Newport 1918-R).

The propagation loss in dB/cm is defined by

$$\text{loss} = -\frac{1}{L}10\log\frac{P_{\text{out}}}{P_{\text{in}}}. \tag{3}$$

Figure 8 shows the propagation loss measured at 1550 nm of the rib waveguide samples fabricated from the as-deposited and annealed films with different lengths (12 mm, 7 mm, and 3 mm). To avoid the experimental uncertainty and statistical error in the loss measurement, several runs of the measurements were carried out on the waveguide samples and the data of the loss were averaged. The calculated propagation losses in 6 μm wide and 4 μm wide annealed waveguides are 1.91±0.21 dB/cm and 2.13±0.26 dB/cm, respectively. The approximate measurement error indicates that the annealed waveguide exhibits more than 0.4 dB/cm lower propagation losses compared to the waveguide before annealing. The propagation loss increase could be primarily attributed to increasing sidewall scattering as the width decreased from 6 μm to 4 μm. In addition, the coupling losses between lensed fibers and the waveguide could be determined by the intercepts of the fitting line, which was ∼ 7 dB/facet for the waveguide. Presumably, the relatively large coupling loss is the mode mismatch between the waveguide and the lens fiber. The coupling loss can be reduced via several approaches, like polishing the waveguide end surface and adding anti reflection coating.[38–40]

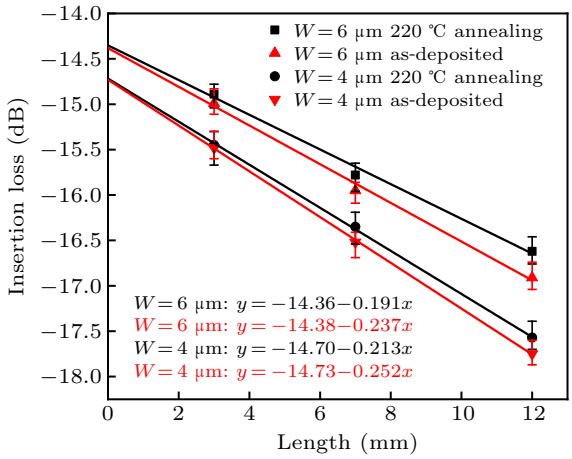


Fig. 8. Insertion loss and propagation loss of waveguides fabricated from the as-deposited and annealed films.

5. Conclusions

In this paper, $Ge_{11}As_{29}S_{25}Se_{35}$ waveguides were fabricated by photolithography and dry etching. The ZDW of the obtained waveguide could be shifted to ∼ 2.1 μm through appropriate dispersion engineering, which provides great convenience for the laser pump wavelength required for SC generation. The experiments demonstrated that thermal annealing is an effective way to reduce film roughness and reduce optical loss. Without changing the geometry of the waveguide cross-section, thermal treatment can reduce film roughness (up to 18%) and reduce optical loss (up to 19%). The corresponding propagation losses of the annealed waveguides of 6 μm (width)×3.5 μm (height) and 4 μm (width)×3.5 μm (height) are 1.9±0.21 dB/cm and 2.13±0.26 dB/cm at 1550 nm, respectively. Based on the optimized design and fabrication process of the waveguide, GeAsSeS chalcogenide waveguides are suitable for potential applications related with SC sources.

References

[1] Dudley J M and Taylor J R 2010 *Supercontinuum Generation in Optical Fibers* (Cambridge: Cambridge University Press)
[2] Colley C S, Hebden J C, Delpy D T, Cambrey A D, Brown R A, Zibik E A, Ng W H, Wilson L R and Cockburn J W 2007 *Rev. Sci. Instrum.* **78** 123108
[3] Guo B, Wang Y, Peng C, Zhang H L, Luo G P, Le H Q, Gmachl C, Sivco D L, Peabody M L and Cho A Y 2004 *Opt. Express* **12** 208

[4] Zhang L, Huang X, Fan X, He W, Yang C and Wang C 2019 *Environ. Technol.* **42** 270
[5] Vainio M and Karhu J 2017 *Opt Express* **25** 4190
[6] Abeeluck A K and Headley C 2005 *Opt. Lett.* **30** 61
[7] Yu Y, Gai X, Ma P, Vu K, Yang Z, Wang R, Choi D Y, Madden S and Luther-Davies B 2016 *Opt. Lett.* **41** 958
[8] Hsieh I W, Chen X, Dadap J I, Panoiu N C, Osgood R M, McNab S J and Vlasov Y A 2006 *Opt. Express* **14** 12380
[9] Christensen S, Rao D S S, Bang O and Bache M 2019 *J. Opt. Soc. Am. B* **36** A131
[10] Gai X, Madden S, Choi D Y, Bulla D and Luther-Davies B 2010 *Opt. Express* **18** 18866
[11] Eggleton B J, Luther-Davies B and Richardson K 2011 *Nat. Photonics* **5** 141
[12] Lucas J 1999 *Curr. Opin. Solid State Mater. Sci.* **4** 181
[13] Yin L and Agrawal G 2007 *Opt. Lett.* **32** 2031
[14] Wang T, Gai X, Wei W, Wang R, Yang Z, Shen X, Madden S and Luther-Davies B 2014 *Opt. Mater. Express* **4** 1011
[15] Yeom D I, Magi E, Lamont M, Roelens M, Fu L and Eggleton B 2008 *Opt. Lett.* **33** 660
[16] Harbold J M, Ilday F Ö, Wise F W, Sanghera J S, Nguyen V Q, Shaw L B and Aggarwal I D 2002 *Opt. Lett.* **27** 119
[17] Quémard C, Smektala F, Couderc V, Barthélémy A and Lucas J 2001 *J. Phys. Chem. Solids* **62** 1435
[18] Petit L, Carlie N, Chen H, Gaylord S, Massera J, Boudebs G, Hu J, Agarwal A, Kimerling L and Richardson K 2009 *J. Solid State Chem.* **182** 2756
[19] Smektala F, Quemard C, Leneindre L, Lucas J, Barthélémy A and Angelis C D 1998 *J. Non-Cryst. Solids* **239** 139
[20] Karim M R, Rahman B M A and Agrawal G P 2015 *Opt. Express* **23** 6903
[21] Karim M R and Rahman B M A 2016 *Opt. Quantum Electron.* **48** 174
[22] Zhang X, Hu H, Li W and Dutta N K 2016 *J. Mod. Opt.* **63** 1965
[23] Estevez M C, Alvarez M and Lechuga L M 2012 *Laser Photonics Rev.* **6** 463
[24] Zhang W, Dai S, Shen X, Chen Y, Zhao S, Lin C, Zhang L and Bai J 2013 *Mater. Lett.* **98** 42
[25] Zuo H, Yu S, Gu T and Hu J 2019 *Opt. Express* **27** 11152
[26] Su X, Wang R, Luther-Davies B and Wang L 2013 *Appl. Phys. A* **113** 575
[27] Wang R, Yan K, Yang Z and Luther-Davies B 2015 *J. Non-Cryst. Solids* **427** 16
[28] Zhao Z, Chen P, Wang X, Xue Z, Tian Y, Jiao K, Wang X g, Peng X, Zhang P, Shen X, Dai S, Nie Q and Wang R 2019 *J. Am. Ceram. Soc.* **102** 5172
[29] Singh S T, Phuoc T H N, Kenshiro N, Xing L, Hoang T T, Takenobu S and Yasutake O 2018 *Appl. Opt.* **57** 1689
[30] Ahmad H, Karim M R and Rahman B M A 2018 *Appl. Phys. B* **124** 47
[31] Gai X, Choi D Y, Madden S, Yang Z, Wang R and Luther-Davies B 2012 *Opt. Lett.* **37** 3870
[32] Zakery A, Ruan Y, Rode A V, Samoc M and Luther-Davies B 2003 *J. Opt. Soc. Am. B* **20** 1844
[33] Bryce R, Nguyen H, Ponnampalam N, DeCorby R, Dewedi P, Haugen C, McMullin J and Kasap S 2004 *J. Vac. Sci Technol. A* **22** 1044
[34] Guo P, Li C, Huang W, Zhang W, Zhang P and Xu T 2020 *Opt. Mater. Express* **10** 129
[35] Choi D Y, Madden S, Bulla D, Wang R, Rode A and Luther-Davies B 2010 *J. Appl. Phys.* **107** 053106
[36] Zhao Y, Li C, Guo P, Zhang W, Xu P and Zhang P 2019 *Opt. Mater.* **92** 206
[37] Fan Z, Yan K, Zhang L, Qin J, Chen J, Wang R and Shen X 2020 *Appl. Opt.* **59** 1564
[38] Wu G, Mirza A R, Gamage S K, Ukrainczyk L, Shashidhar N, Wruck G and Ruda M 2004 *J. Micromech. Microeng.* **14** 1367
[39] Choi C G, Han Y T, Kim J T and Schift H J A P L 2007 *Appl. Phys. Lett.* **90** 221109
[40] Nguyen M H, Chang C J, Lee M C and Tseng F G 2011 *Opt. Express* **19** 18956